PAPER

Superior properties and behaviour of coatings produced on nanostructured titanium by PEO coupled with the EPD process

To cite this article: Lokeshkumar E *et al* 2022 *Surf. Topogr.: Metrol. Prop.* **10** 015020

Surface Topography: Metrology and Properties

RECEIVED
23 December 2021

REVISED
1 February 2022

ACCEPTED FOR PUBLICATION
4 February 2022

PUBLISHED
18 February 2022

PAPER

Superior properties and behaviour of coatings produced on nanostructured titanium by PEO coupled with the EPD process

Lokeshkumar E[1], Saikiran A[1,2], B Ravisankar[1], Rama Krishna L[3], Parfenova L V[4,5], Parfenov E V[5], Valiev R Z[5] and Rameshbabu N[1]

[1] Department of Metallurgical and Materials Engineering, National Institute of Technology, Tiruchirappalli 620015, India
[2] School of Marine Engineering and Technology, Indian Maritime University, Chennai 600119, India
[3] Centre for Engineered Coatings, International Advanced Research Centre for Powder Metallurgy and New Materials (ARCI), Hyderabad 500005, India
[4] Institute of Petrochemistry and Catalysis, Russian Academy of Sciences, Ufa 450075, Russia
[5] Ufa State Aviation Technical University, Ufa 450008, Russia

E-mail: nrb@nitt.edu

Keywords: nanostructured titanium, PEO-EPD process, L-929 cell, corrosion resistance, cytotoxicity, apoptosis

Abstract

Surface modification of commercially pure Grade 4 coarse-grained titanium (CG-Ti) and nano-grained titanium (n-Ti) by plasma electrolytic oxidation (PEO) and plasma electrolytic oxidation conjugated with electrophoretic deposition (PEO-EPD) processes is reported in the present study. Two different coatings were developed on each CG-Ti and n-Ti in phosphate-based electrolytes without and with the incorporation of hydroxyapatite (HA) nanoparticles. The phase composition, morphology (surface and cross-sectional), corrosion resistance, surface roughness, and scratch-resistance of the fabricated coatings were thoroughly studied and analysed. The L-929 fibroblast cells were used for assessing the *in-vitro* cell viability. The L-929 cells cultured on PEO-EPD treated CG-Ti, and n-Ti samples exhibited higher cell growth than PEO treated CG-Ti and n-Ti samples. Among all the PEO and PEO-EPD treated samples, the PEO-EPD treated n-Ti sample showed significantly better corrosion resistance ($i_{corr} = 8.85 \times 10^{-7}$ mA cm^{-2}), lower contact angle (40°), and good adhesion strength ($L_c = 29$ N), demonstrating the importance of the nanostructuring of the titanium substrate for the properties of the coating. The origin of the discovered enhancement in the properties of the modified PEO coating produced on nanostructured titanium was examined and discussed. After soaking in SBF for 14 days, the PEO-EPD treated sample is wholly covered with apatite layer indicating its good bioactivity

1. Introduction

Metallic materials are widely used for load-bearing medical implant applications like orthopaedics, artificial joints, bone screws, and dentistry. Metallic materials intended for usage in medical implant applications should comply with specific criteria like biocompatibility, corrosion-resistance, and non-toxicity to the body fluid environment apart from possessing ample mechanical strength and toughness [1, 2]. Hence, Cobalt-chromium (Co-Cr) alloys, stainless steels (SS), titanium, and its alloys are typically used for biomedical implants. Among these, titanium and its alloys are gaining a lot of attention towards using hard tissue replacements in artificial joints, bones, and dental implants due to their low elastic modulus and better biocompatibility than the other metallic implant materials. Titanium's lower elastic modulus (value) results in a significantly smaller stress shielding effect between the bone and implanted material than the other implant materials [3]. However, commercially pure (CP) titanium has relatively lower mechanical strength than the other metals used in biomedical implants. The strength of titanium can be improved by either alloying or secondary processing like rolling, drawing, equal channel angular pressing, etc. The addition of alloying elements to CP titanium allows for a considerable improvement of the mechanical properties. But the addition of typical alloying elements such as vanadium and aluminium increases the toxicity due to the release of the corresponding metal ions into the body fluid over a prolonged period. Therefore, much effort is being directed towards developing Al and V free

Ti alloys [4]. Strengthening by mechanical working processes like rolling, drawing, etc, can be achieved. The physical and mechanical properties of implant materials can be improved significantly with a reduction in grain size. Hence, attention has been increasing to produce materials with extremely small grain sizes nowadays. Researchers have been developing nanostructured materials by grain size reduction for the last two decades, which is an efficient way to enhance its physicomechanical properties than coarse-grain structured materials [5, 6]. From the recent studies on developing nanostructured titanium implants by severe plastic deformation (SPD), it is palpable that a considerable improvement in the mechanical properties has been observed apart from the enhancement in the biocompatibility and osseointegration [7, 8]. Commercially available coarse-grained titanium exhibits ultimate tensile strength and yield strength of ∼700 MPa and ∼530 MPa, respectively. The equal channel angular pressing via 'Conform' (ECAP-C) is a quite efficient method to enhance the mechanical properties of titanium. It is reported to exhibit ultimate tensile strength and yield strength ranging from ∼1200–1300 MPa and ∼1100–1150 MPa, respectively [9]. Nanostructured titanium was reported to exhibit an improved corrosion resistance attributed to developing a strong passive film at grain boundaries and the absence of impurity segregation [10–12]. Fattah-alhosseini *et al* documented that formed passive oxide films on the nano-grained titanium samples resulted in attaining better corrosion resistance than coarse-grained titanium in Ringer's physiological solution [13]. Titanium and titanium alloys have naturally formed thin oxide film (∼1.5–10 nm) but may deteriorate during load-bearing applications due to their low thickness and amorphous nature. Hence the unprotective metallic titanium substrate gets corroded in physiological environments, releasing metal ions from the implant surface. The corrosion products accumulated at surrounding tissues can cause inflammatory responses. Hence, the corrosion rate of the titanium material has to be mitigated for the effective biological performance and attainment of the extended service life of the implant [14]. However, surface modification of nanograined titanium is essential to enhance further its corrosion resistance and augmentation of biocompatibility, cell viability, bioactivity, and cell adhesion. Various surface modification techniques like hot-dipping, sol-gel deposition, selective laser melting, plasma spray, and electrochemical processes prevail. Among these techniques, electrochemical modification processes like anodisation and plasma electrolytic oxidation (PEO) are cost-effective, eco-friendly, and the simplest processes [15]. Semenova *et al* documented those coatings produced on ultrafine-grained titanium (UFG Ti) exhibited considerable improvement in the adhesive strength and hardness due to a greater number of propagation and growth points in the coating development process and compact coatings produced than the CG-Ti [16]. Thick and highly adherent oxide coatings can be produced on Mg, Ti, Zr, Al, Nb, and their alloys by the PEO process [17–21]. Manojkumar *et al* developed a uniform and thicker titanium oxide (TiO_2) coating on CP-Ti by PEO process using phosphate-based electrolytes and reported that the coated samples exhibited superior corrosion resistance than substrate [22]. Xu *et al* studied the influence of process time (3, 6, 9, 12, and 15 min) on the characteristics and bioactivity of PEO coatings developed on ultrafine-grained Ti using silicate and phosphate-based mixed aqueous solution. They suggested that the sample PEO coated over 9 min duration has evinced the superior adhesion and proliferation of the osteoblast cells [23]. Yao *et al* reported that relatively thicker titanium oxide coatings could be developed on equal channel angular pressed titanium (ECAPed Ti) samples compared to the coarse-grained Ti samples by micro-arc oxidation (MAO) process [24]. PEO coatings are porous and thereby promote bone tissue maturity and reduce osteointegration time. The biological properties like bioactivity, viability, and proliferation of the cells on the implants can be augmented by blending the electrolytes with hydroxyapatite (HA) nanoparticles by virtue of the similar composition of HA to the mineral part of the bone besides the existence of crystal defects and relatively higher specific surface area [25–29]. Liu *et al* produced nanostructured HA coatings on CP-Ti via chemical conversion method. They inferred that coatings had a better scratch and wear resistance and superior corrosion-resistant properties [30]. In recent years, electrophoretic deposition (EPD) has been accomplished as an interesting technique to develop composite coatings by migration of charged ceramic particles towards opposite polarity electrode under the influence of an electric field. A recent study successfully combined the EPD technique with anodisation to prepare a corrosion-resistant Ta_2O_5/Mn_3O_4 coating on tantalum [31]. A novel MgO-Graphene oxide (GO) duplex coating was produced on AZ91 Mg alloy by PEO process followed by EPD process with GO platelets [32]. Corrosion-resistant and bioactive duplex coatings are produced on plasma electrolytic oxidised AZ91 magnesium alloy by developing a pore-sealing layer consisting of ZnO nanoparticles by the EPD method [33]. However, to the best of the authors' knowledge, no work had documented the influence of HA nanoparticle inclusion on the cytocompatibility and corrosion resistance properties of PEO and PEO-EPD coatings fabricated on coarse-grained CP-Ti and nanostructured titanium.

The present work aims to fabricate Ca and P containing titanium oxide (TiO_2) coatings on coarse-grained and nanostructured commercially pure titanium by PEO and PEO-EPD processes with and without HA nanoparticles' inclusion to the phosphate-based electrolyte. The phase composition of the synthesised coatings was appraised by the XRD technique. Morphological analysis of the coatings along the surface and cross-section, with the surface elemental analysis, was assessed by FESEM furnished with EDS. The

Table 1. Identification codes for the coatings along with the detailed composition of electrolytes, conductivity (k), breakdown (V_b), and final voltages (V_f).

Sl. No.	Sample code	Electrolyte concentration (g l^{-1})	k (mS cm^{-1})	V_b (±2 V) (V)	V_f (±2 V) (V)
1	CT-PEO	5 g $Na_3PO_4.12H_2O$ + 2 g KOH	11.32	294	454
2	CT-EPD	5 g $Na_3PO_4.12H_2O$ + 2 g KOH + 5 g HA	10.25	324	482
3	NT-PEO	5 g $Na_3PO_4.12H_2O$ + 2 g KOH	11.32	314	465
4	NT-EPD	5 g $Na_3PO_4.12H_2O$ + 2 g KOH + 5 g HA	10.25	336	491

wettability and corrosion behaviour of the coated samples were evaluated. MTT assay, apoptosis, and direct contact tests were performed to evaluate the cell (L-929) viability of the substrate and coated specimens.

2. Materials and methods

2.1. Fabrication of coatings

Commercially pure Grade 4 coarse-grained titanium (CG-Ti) cylindrical pellets of 4 mm thickness and 10 mm diameter were used as CG-Ti substrates. Conventional CG-Ti was processed at 200 °C using the angular channel of 120° by equal channel angular pressing via 'Conform' processing (ECAP-C) to produce nanostructured titanium. The processed material is used as nanostructured titanium (n-Ti) substrate as a pellet with a diameter of 8 mm and 3 mm thickness. The CG-Ti and n-Ti samples exhibited an average grain size of 25 μm and 100–150 nm, respectively [34]. The titanium metal pellets were polished with various grit sizes of 400, 600, 800, 1000, and 1200 silicon carbide (SiC) papers, followed by alumina polishing. Subsequently, the surface of the pellets was made contaminant-free by cleaning with acetone followed by flushing with double distilled water and air drying before the inception of the coating process.

Fabrication of titanium oxide (TiO_2) films on CG-Ti and nanostructured titanium by PEO was carried out using a pulsed DC power unit (Milman, India). The aqueous electrolyte solution with 5 g trisodium orthophosphate (TSOP; $Na_3PO_4{\cdot}12H_2O$) + 2 g KOH in 1 l distilled water was used for developing PEO coatings. TiO_2 containing Ca and P were developed on titanium by an innovative method based on PEO-EPD by blending the base electrolyte with 5 g l^{-1} HA ($Ca_{10}(PO_4)_6OH_2$) nanoparticles. The nanosized HA particles with average longitudinal and transverse dimensions of 70 nm and 20 nm produced by the microwave synthesis method were used in this study [26]. Prior to the PEO-EPD process, the electrolyte was supplemented with 5 ml ethylene glycol to charge HA nanoparticles and 10 ml triethanolamine suspension to stabilise the electrolyte. The electrolyte was then sonicated with an ultrasonic vibrator for 45 min to attain homogeneity. The stainless-steel bowl accommodates electrolyte, was used as a cathode, and titanium pellets connected with aluminium foil were used as an anode. The electrolyte bath was retained at room temperatures (30 °C–40 °C) during the process by circulating chilled water. All the coatings were produced under similar electrical conditions of 1000 Hz frequency and 90% duty cycle with a current density of 150 mA cm^{-2} during 6 min of coating duration. The identification codes for coarse-grained titanium and nanostructured titanium were indicated by CG-Ti and n-Ti, respectively, and the sample codes of both PEO-EPD and PEO coated samples are stated in table 1. The CT and NT in coated sample codes indicate the coarse-grained Ti and Nano-grained Ti, respectively. Hereafter, titanium substrates and all the coatings are reported with their respective identification codes. The composition and conductivity of the prepared phosphate electrolytes along with the final voltages (V_f) and breakdown (V_b) recorded during the process, are represented in table 1.

2.2. Evaluation of the PEO and PEO-EPD coatings

The phases present in the PEO treated titanium samples were analysed by documenting the diffraction pattern spanning over a 2θ range of 10°–90° with an interval of 0.05° at a scan speed of 1° min^{-1} using an x-ray diffraction unit (XRD, Rigaku Ultima IV) functioning at 30 mA and 40 kV and emitting Cu Kα radiation (1.5406 A°).

The surface morphology, elemental composition, and coating thickness of the PEO and PEO-EPD coated titanium samples were appraised by field emission scanning electron microscope (FESEM, Zeiss Gemini-300) equipped with an energy dispersive x-ray spectrometer (EDS, EDAX). The thickness of the coatings was gauged at five distinct spots along the cross-section using FESEM cross-sectional micrographs, and the average values were reported. The coating thickness values were also substantiated by gauging with an eddy current thickness gauge. The average surface roughness of PEO treated samples was evaluated over the surface area of 0.8 × 0.8 mm using Taylor Hobson made Talysurf CCI with horizontal and vertical resolution limits of 300 nm and 0.1 nm, respectively.

An automatic scratch tester equipped with a stylus of a 200 μm radius (Revtest CSM Instruments) was employed to assess the practical adhesion strength of the coatings. Scratch tracks were made over a track length of 5 mm under the progressive loading condition from 1 N to 40 N at a rampage rate of

19.5 N min^{-1}, and the obtained scratch tracks were captured with an optical microscope.

Contact angle goniometer (DSA100, KRUSS) was used to assess the wettability of titanium substrates and coated samples by using a sessile 3 μl water droplet. The test was performed at ten various locations on the individual sample by measuring the contact angle with the aid of images captured by the camera, and the corresponding average values were reported.

The corrosion characteristics of titanium substrates, PEO and PEO-EPD samples in the simulated body fluid (SBF) were assessed by Potentiodynamic polarisation (PDP) technique with the aid of a potentiostat (Gill AC model, ACM instruments, UK) constituting sample of interest as a working electrode and polarising it from anodic side −500 mV to cathodic side up to +3000 mV with reference to the open circuit potential (OCP) at a rampage rate of 0.166 mV s^{-1}. A saturated calomel electrode (SCE) was used as a reference electrode along with an auxiliary platinum electrode. The simulated body fluid was prepared by abiding by Kokubo's protocol [17], and it is used for the PDP test by exposing a sample surface area of 1 cm^2. The electrochemical corrosion tests were repeated thrice for assuring the results reported.

2.3. *In vitro* assessment of cytotoxicity

2.3.1. Direct contact assay and MTT assay

The fibroblast L-929 cells were used to evaluate the cytotoxicity and cell proliferation on both coarse-grained, nanostructured titanium substrate and coated samples. The substrates (CG-Ti, n-Ti), PEO coated samples (CT-PEO, NT-PEO), and PEO-EPD samples (CT-EPD, NT-EPD) were submerged into the well plates seeded with cells of sufficient confluence (~70%–80%) after irradiating under ultraviolet (UV) light for 1 h. The submerged samples were then granted to incubate for the next 24 h. After the incubation period, aggregation and growth of the L-929 cells abutting the samples were assessed by analysing the morphological changes using an inverted phase-contrast microscope.

The mitochondrial cellular metabolism (viability) was assessed by using MTT (3-[4,5-dimethylthiazole-2-yl]-2,5-diphenyltetrazolium bromide solution) assay. The percentage viability of the cultured fibroblast cells was gauged by measuring the optical density (OD) at 540 nm using the coloured solution. A standard MTT assay procedure was followed, as mentioned in our previous work [20]. The viability percentage was evaluated based on the optical density (OD) according to the following equation, in which cultured cells without a sample was considered as control.

$$\%\text{Viability} = \frac{OD\ \ of\ \ test}{OD\ \ of\ \ control} \times 100 \qquad (1)$$

2.3.2. Apoptosis test

The titanium substrates (CG-Ti, n-Ti), PEO coated samples (CT-PEO, NT-PEO) and PEO-EPD samples (CT-EPD, NT-EPD) were placed in cell culture well plates and allowed to be incubated for 24 h. The well plates were cleaned with phosphate-buffered saline (PBS), followed by adding a blend of ethidium bromide (EtBr, 100 mg ml^{-1}) and acridine orange (AO, 100 mg ml^{-1}). Ethidium bromide was absorbed by non-viable cells, and the acridine orange was absorbed by both non-viable and viable cells. Then samples were ascertained with fluorescent microscope's blue filter; prior to that, stained cells were cleaned thrice using PBS.

2.4. *In-vitro* bioactivity study

The apatite forming ability of CT-PEO, CT-EPD, NT-PEO, and NT-EPD samples was evaluated by immersing the samples in 7.4 pH SBF for 14 days in separate plastic vials. The ratio of the surface area [in mm^2] of immersed sample to SBF solution (in ml) volume was set equal to 10. Every 24 h, the SBF solution was renewed and kept stable. The samples were taken out from the SBF after 14 days, gently rinsed with distilled water, dried in air and finally characterised by FESEM.

3. Results and discussion

3.1. Coating growth mechanism

The voltage-time (V-T) response graphs of both PEO and PEO-EPD processes for the two electrolytes employed to coat coarse-grained and nanostructured titanium are depicted in figure 1. The coating process was operated in constant current mode, and hence process voltage increases with process time and reaches a constant value. The process can be mainly divided into three regimes based on process voltage behaviour, namely anodisation stage, dynamic PEO (sparking) stage and near steady stage PEO (arcing) stage. In the anodisation region, the process voltage increases linearly up to the first inflection point (breakdown voltage, V_b), and there were no sparks observed in this region. The next region is between the breakdown voltage and critical voltage (second inflection point), having a lower voltage rate, and tiny white sparks were observed during this regime. In the third stage of PEO, after critical voltage where the process voltage rate gets quasi-stabilised and reaches a peak value (V_f), where the tiny white sparks were converted to sizeable orange colour sparks with low spatial density. The developed orange colour sparks appeared till the end of the PEO process. The breakdown voltages (V_b) and final voltages (V_f) of the PEO and PEO-EPD processes are recorded and mentioned in table 1. The recorded breakdown voltages of coated samples CT-PEO, CT-EPD, NT-PEO, and NT-EPD are 294, 324, 314, and 336 V, respectively. The nanostructured titanium samples exhibited higher breakdown voltages than the coarse-grained titanium during the coating process. Also, PEO-EPD processed samples (CT-EPD and NT-EPD) recorded higher breakdown voltages as compared to PEO samples

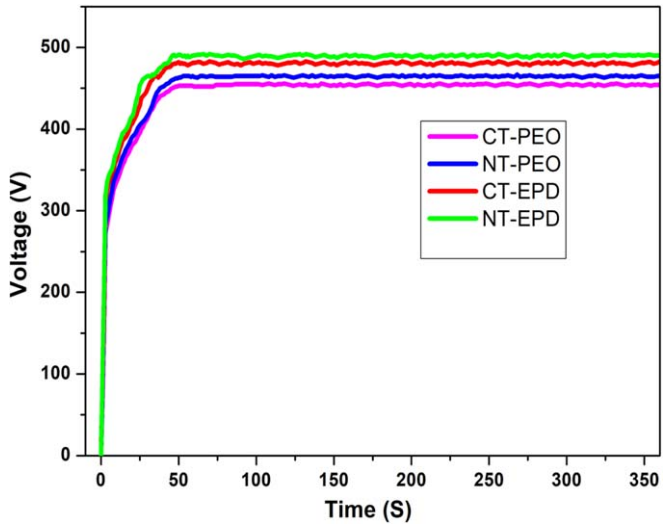

Figure 1. Voltage-time response curves for PEO and PEO-EPD coatings.

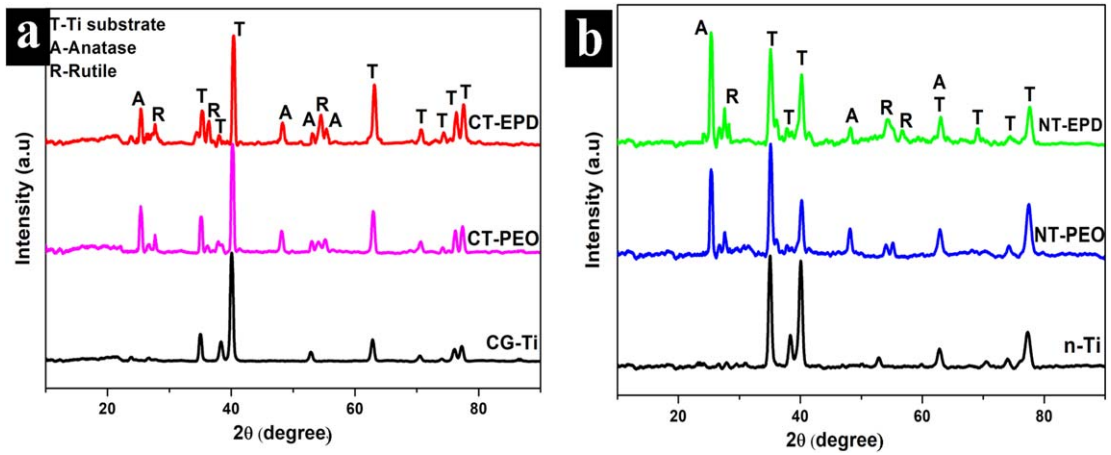

Figure 2. XRD patterns of (a) CG-Ti, CT-PEO and CT-EPD, (b) n-Ti, NT-PEO and NT-EPD.

(CT-PEO and NT-PEO). These higher breakdown voltages of PEO-EPD samples might be due to the lower conductivity of the electrolytes used for PEO-EPD samples compared to those for the PEO process, as it abides by Ikonopisov's model [35].

3.2. Phase analysis of coatings

The XRD patterns of coarse-grained titanium substrate and its coatings (CT-PEO, CT-EPD), nanostructured titanium, and its coatings (NT-PEO, NT-EPD) are reported in figures 2(a) and (b), respectively. Diffraction patterns of all the coated samples exhibited substrate peaks in addition to characteristic peaks of both crystalline anatase (at $2\theta \sim 25.3°$, JCPDS: 21-1272) and rutile (at $2\theta \sim 27.7°$, JCPDS: 21-1276) forms of titanium oxide (TiO_2). The characteristic titanium peak intensity present at $2\theta \sim 35°$ for nanostructured titanium is stronger compared to the coarse-grained titanium, which agrees with the Kim *et al* research work [12]. The relative amount of anatase and rutile phases of PEO treated samples can be calculated by the following formulae and reported in table 2:

Table 2. Anatase and rutile phase composition of the PEO and PEO-EPD coated samples.

Sample	Anatase (wt. %)	Rutile (wt. %)
CT-PEO	61.15	38.85
CT-EPD	66.28	33.72
NT-PEO	74.85	25.15
NT-EPD	78.42	21.58

$$X_A = \frac{1}{1 + 1.26 \quad (\frac{I_R}{I_A})} \tag{2}$$

and

$$X_R = \frac{1}{1 + 1.26 \quad (\frac{I_A}{I_R})} \tag{3}$$

where I_R and I_A have reported the characteristic peak intensities of rutile ad anatase phases, respectively. The

PEO and PEO-EPD coatings consist of both anatase and stable rutile phases. During the PEO process, the temperature in discharge channels is >3000 K producing TiO_2 in a molten state, and the molten oxide is rapidly quenched by the electrolyte at room temperature forming amorphous titania. On recurrent heating by the subsequent plasma discharges, the amorphous TiO_2 in coatings converts to crystalline anatase and subsequently transforms partially to the rutile phase. The metastable anatase changes to rutile at a temperature above 610 °C, and the transition completes by 915 °C [36]. Titania formed by the plasma discharges at the end of the PEO process can be retained as an amorphous phase. Thus, the percentage of crystalline anatase and rutile phases and amorphous phase depends on the thermal history of the phases formed in coatings. The anatase content in the coated samples is 61.15%, 66.28%, 74.85%, and 78.42% for CT-PEO, CT-EPD, NT-PEO, and NT-EPD, respectively. The samples NT-PEO and NT-EPD have higher anatase phase % than the CT-PEO and CT-EPD, respectively. HA nanoparticle incorporated PEO-EPD samples improved the anatase phase % as compared to PEO treated samples. The NT-EPD sample having more anatase phase among all the samples plays a crucial role to enhance biological properties like osteoblast cell proliferation, cell adhesion, and cell growth [37]. The absence of diffraction peaks corresponding to the HA phase in the XRD patterns of PEO-EPD coated coarse-grained and nanostructured titanium samples might be owed to the minute levels of HA incorporation into discharge channels or due to the presence of re-solidified amorphous [26]. Yet, elements Ca, and P were ensured from the elemental analysis as discoursed in section 3.3.

3.3. Surface morphology, elemental composition, and cross-section of coatings

The FESEM micrographs illustrating the surface morphology of PEO and PEO-EPD coatings on CG-Ti and n-Ti substrates, accompanied by the elemental compositions, are portrayed in figure 3. All the micrographs of titanium coated samples displayed porous structure, which is the peculiarity of the films developed by the PEO process. However, significant variation in their surface morphology is evident with the substrate and electrolyte composition in variation. The surface micrographs of PEO treated samples (CT-PEO, NT-PEO) exhibited fewer pores than PEO-EPD samples (CT-EPD, NT-EPD). The developed PEO coated samples have large size interconnected pores. In contrast, PEO-EPD samples exhibited comparatively isolated and a greater number of roughly circular or elliptical tiny pores distributed uniformly throughout the surface. It represents that HA particle addition influenced the morphology in terms of reducing pore size [20]. Discharge channels (pores) present in CG-Ti coatings are significantly smaller in size as compared to n-Ti coatings. A similar observation made by Yao *et al* states that discharge channel diameter, surface roughness, and thickness of PEO coatings developed on CG-Ti is significantly smaller than those on n-Ti coatings [24].

The EDS spectra of coated samples CT-PEO, CT-EPD, NT-PEO, and NT-EPD are depicted in figure 3, and the respective elemental composition of coatings is stated in table 3. The EDS analyses for coated samples were performed over five different locations on each coated sample, and the average values from the obtained results were considered. From table 3, the atomic percentage of Ti element for PEO-EPD coated films was minimal compared to the PEO sample, attributing to the produced coating higher thickness and compactness. From figure 3, we observe that PEO treated samples (CT-PEO and NT-PEO) contain Ti, O, P elements. But PEO-EPD samples (CT-EPD and NT-EPD) consist of Ca, and P in addition to Ti and O attributed to the effective reactive incorporation of HA nanoparticles into the coating. The Ca/P ratios for samples CT-EPD and NT-EPD are 1.51 and 1.62, respectively.

The cross-sectional micrographs of CT-PEO, CT-EPD, NT-PEO, and NT-EPD samples are displayed in figure 4, from which the average coating thickness is assessed and reported in table 4. The PEO treated CT-PEO and NT-PEO samples exhibited more porous and relatively less compact coatings with lower thickness compared to the PEO-EPD samples. The PEO-EPD treated CT-EPD and NT-EPD samples showed highly compact coatings with higher thickness compared to PEO treated samples. Nanostructured Ti samples offer thicker and more compact coatings compared to CG-Ti coatings. The chemical reaction of an n-Ti substrate could enhance due to high energy grain boundaries, leading to the formation of thicker oxide film [38]. Among all the PEO and PEO-EPD coatings, the NT-EPD sample reported a higher coating thickness ($14.5 \pm 1\ \mu$m).

3.4. Surface roughness and depth profile of coatings

The 3D surface topography and surface roughness (R_a) of the fabricated samples CT-PEO, CT-EPD, NT-PEO, and NT-EPD have been studied by an optical profilometer. A square area of 0.8 mm × 0.8 mm has been scanned to obtain 3D surface topographical images. Usually, the surface roughness of PEO coated samples is mainly affected by pore nature (deep or shallow), pore size, pore density, pinholes, and microcracks. The 3D surface topographical images are reported in figure 5. From figure 5, the hills indicated that upraised regions (pancake projections) over the nominal surface level of the fabricated coatings developed during the PEO and PEO-EPD process. The valley regions report the distribution of shallow and deeper pores present on the coated sample surface. The crest portions appear red, and the deeper pits seem to be blue. The CG-Ti coated samples have significantly lower surface roughness values as

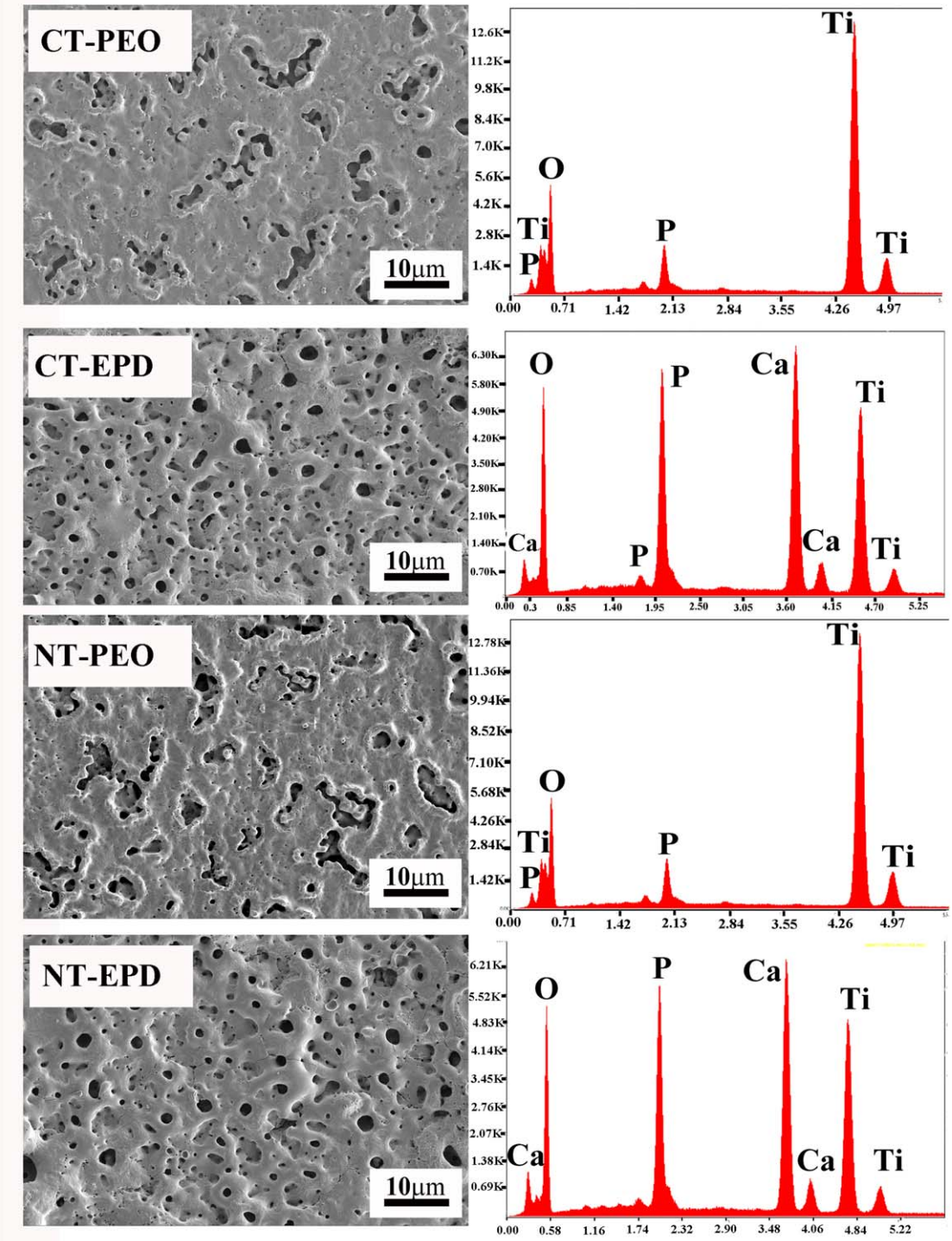

Figure 3. FESEM surface morphology and EDS spectra of PEO and PEO-EPD coated samples.

compared to n-Ti coated samples. The PEO coated samples exhibited more red and blue portions spread throughout the surface, indicating the rough nature of the surface. In contrast, PEO-EPD samples consist of a fewer number of crests and troughs. This clearly indicates PEO-EPD samples have lower surface roughness values than PEO treated samples since pores are sealed with hydroxyapatite (HA) nanoparticles in the PEO-EPD process [20]. The deviation of a surface profile from the mean line represents the surface roughness (R_a). The coated titanium samples R_a values are reported in table 4. Depth profiles of all the coated samples are portrayed in figure 6. The depth profiles of PEO-EPD samples exhibited fewer crests and troughs than PEO treated samples, which corroborates with the coated titanium surface micrographs and their 3D surface profiles. The biomedical implants are expected to display favourable cell proliferation and response when surface roughness values are plotted between 0.4 and 3.5 μm. The R_a values obtained for all the coated

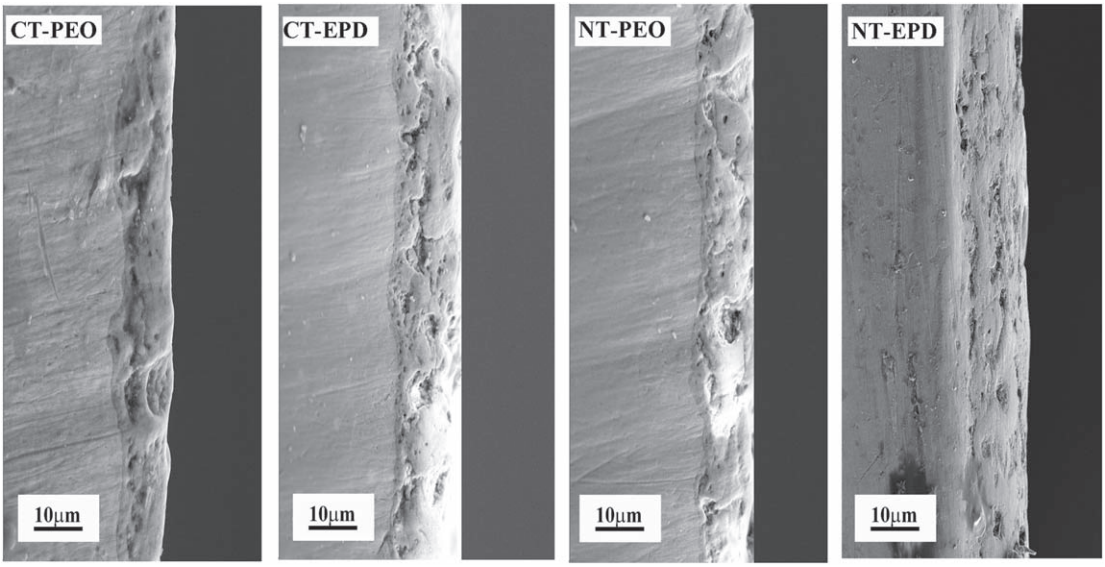

Figure 4. FESEM cross-section images of the PEO and PEO-EPD coated samples.

Table 3. Elemental composition of the PEO and PEO-EPD coated samples.

Sample code	CT-PEO (at.%)	CT-EPD (at.%)	NT-PEO (at.%)	NT-EPD (at.%)
O	69.70	65.63	69.47	65.62
Ti	26.97	9.91	27.10	11.94
P	3.33	9.71	3.43	8.56
Ca	—	14.75	—	13.88

Table 4. Coating thickness (t), surface roughness (R_a) of PEO and PEO-EPD coated samples.

Sample	t (μm)	R_a (μm)
CT-PEO	9 ± 1	2.91 ± 0.1
CT-EPD	12 ± 1	2.03 ± 0.1
NT-PEO	11 ± 1	3.16 ± 0.1
NT-EPD	14.5 ± 1	2.51 ± 0.1

titanium samples were marked within the acceptable range, making them more suitable for biomedical applications [39].

3.5. Wettability study

The wettability of the solid surface is an essential property for biomedical implants, which depends on both the surface geometrical structure and chemical composition [17]. Water droplet images of CG-Ti, n-Ti and coated samples are reported in figure 7 and corresponding average contact angles are reported in table 5. The surface water contact values of CG-Ti, CT-PEO, CT-EPD, n-Ti, NT-PEO, and NT-EPD samples are 74°, 58°, 44°, 71°, 52°, and 40°, respectively. The wettability and capillarity of n-Ti can enhance due to a greater number of grain boundaries on the ECAPed material [40]. The CT-EPD and NT-EPD samples exhibited lower contact values than CT-PEO and NT-PEO samples, respectively. It illustrates that HA nanoparticles incorporation may diminish the contact angle by modifying the surface morphology of PEO-EPD coated samples. All the coated samples reported hydrophilic nature (contact angle $<90°$), which is beneficial for adsorption and interaction of tissue, proteins, and cells for biomaterial implant surfaces. The surface energy (E_s) of all the samples can be evaluated by using the following equation:

$$E_s = E_{vl} \quad \cos\theta \tag{4}$$

where 'θ' represents the contact angle and 'E_{vl}' indicates the surface energy between air and pure water at 20 °C (i.e., 72.8 mJ m^{-2}). The calculated E_s values of all the coated samples along with the substrates are reported in table 5. Usually, higher surface energy metallic implants promote cell adhesion and rapid growth of apatite [17, 26]. The NT-EPD sample showed higher surface energy (56 mJ m^{-2}) and lower contact angle (40°) from these reported values, accomplishing a highly acceptable orthopaedic and dental implant material for attaining superior biological properties like cell spreading and attachment.

3.6. Scratch resistance behaviour of coatings

Adhesion strength is an essential criterion to assess the durability of PEO coatings. The Scratch test is one of the most effective and practical methods for evaluating coatings' adhesion strength. The scratch test was performed over the coating surface by operating with the progressive load, thereby causing plastic deformation until its delamination. The damage might be a cohesive type of failure (chipping within the coating) or an adhesive type of failure (coating spallation). The

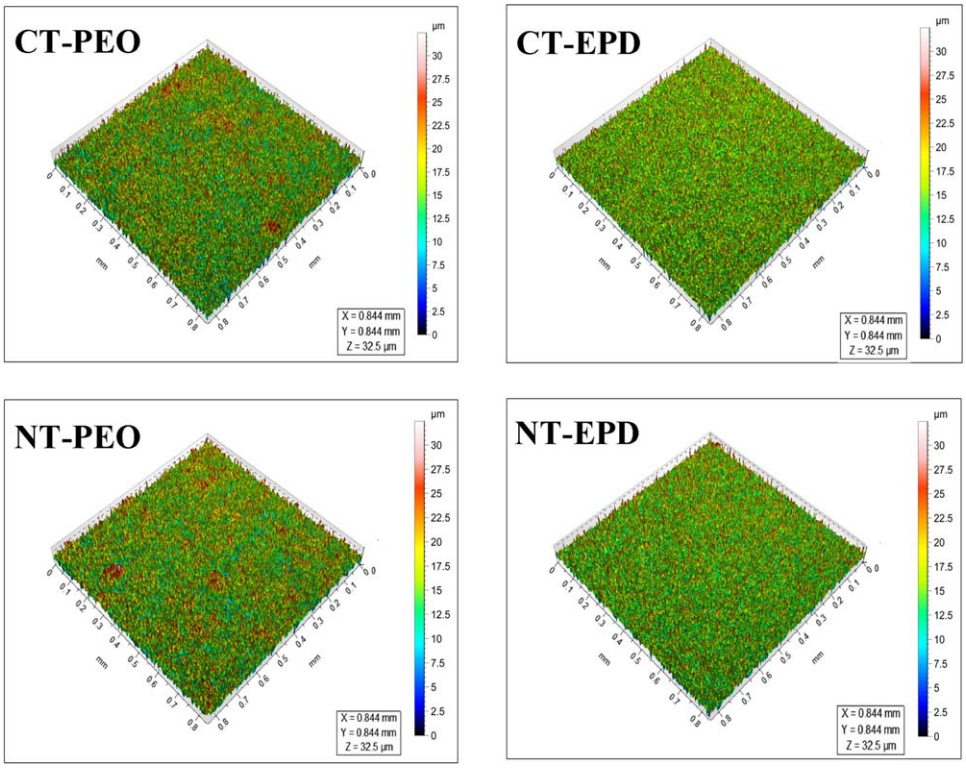

Figure 5. 3D surface profiles of PEO and PEO-EPD coated samples.

load at which delamination of the coating by virtue of adhesive failure leaving the substrate's bright visual is considered critical load (L_c). The L_c of the coated samples relies upon phase composition, the surface morphology of coatings, surface roughness (R_a), and coating thickness [41]. The panoramic view of scratch tracks of the PEO treated samples and their load vs friction force graphs are depicted in figure 8. The critical load of the CT-PEO, CT-EPD, NT-PEO and NT-EPD samples are 19 N, 25 N, 22 N, and 29 N, respectively, and are disclosed in table 5. The CT-EPD and NT-EPD samples recorded higher L_c values than CT-PEO and NT-PEO samples. It can be ascribed to the significantly less porous and compact nature of the coatings produced by PEO-EPD, along with their higher thickness as evident from figures 3 and 4 of surface morphology and cross-section morphology. Moreover, the nanostructured titanium consists of many propagation and growth points present on the substrate. It played a vital role during the coating process and formed dense and compact coating. Due to that, the coatings produced on n-Ti exhibited a higher critical load compared to CG-Ti coatings [16]. A similar trend was observed by Wang *et al* while producing diamond-like carbon (DLC) coatings on UFG-Ti, CG-Ti and Ti-6Al-4V. The UFG-Ti reported significantly higher scratch resistance than CG-Ti and Ti alloy [42]. Among all the coatings, the NT-EPD sample exhibited the superior scratch resistance of 29 N due to its thicker and dense coating.

3.7. Potentiodynamic polarisation (PDP) test

The potentiodynamic polarisation test was used to examine the passivation behaviour of PEO, PEO-EPD coated samples along with CG-Ti and n-Ti substrate. The polarisation curves of the coated samples along with CG-Ti and n-Ti substrates are depicted in figure 9. All the coated samples and substrates mainly showed two regions at the anodic portion, namely the active and passive regions. The corrosion resistance of the samples can be characterised by considering the current density (i_{corr}) and corrosion potential (E_{corr}) which are reported in table 6. The i_{corr} and E_{corr} values of the substrate and the coatings were derived by the Tafel extrapolation method. We have considered both anodic and cathodic curves to evaluate the i_{corr} and E_{corr} values. The Tafel extrapolation was carried out at a linear potential range of $\pm$250 mV with reference to the OCP. The i_{corr} and E_{corr} values were noted from intersection points of the linear portions of both anodic and cathodic curves [36]. The corrosion rate will be represented by current density (i_{corr}), and the thermodynamic tendency will be represented by corrosion potential (E_{corr}). E_{corr} (vs SCE) value of the CG-Ti, CT-PEO, CT-EPD, n-Ti, NT-PEO, and NT-EPD samples are -501.5 mV, -401.2 mV, -353.5 mV, -436.5 mV, -355.9 mV, and 1251.4 mV, respectively, and corresponding i_{corr} values are 1.05×10^{-4} mA cm^{-2}, 2.93×10^{-5} mA cm^{-2}, 1.84×10^{-6} mA cm^{-2}, 3.33×10^{-5} mA cm^{-2}, 3.85×10^{-6} mA cm^{-2}, 8.85×10^{-7} mA cm^{-2}, respectively. The n-Ti produced by ECAP presents superior corrosion resistance than CG-Ti, which might be due to

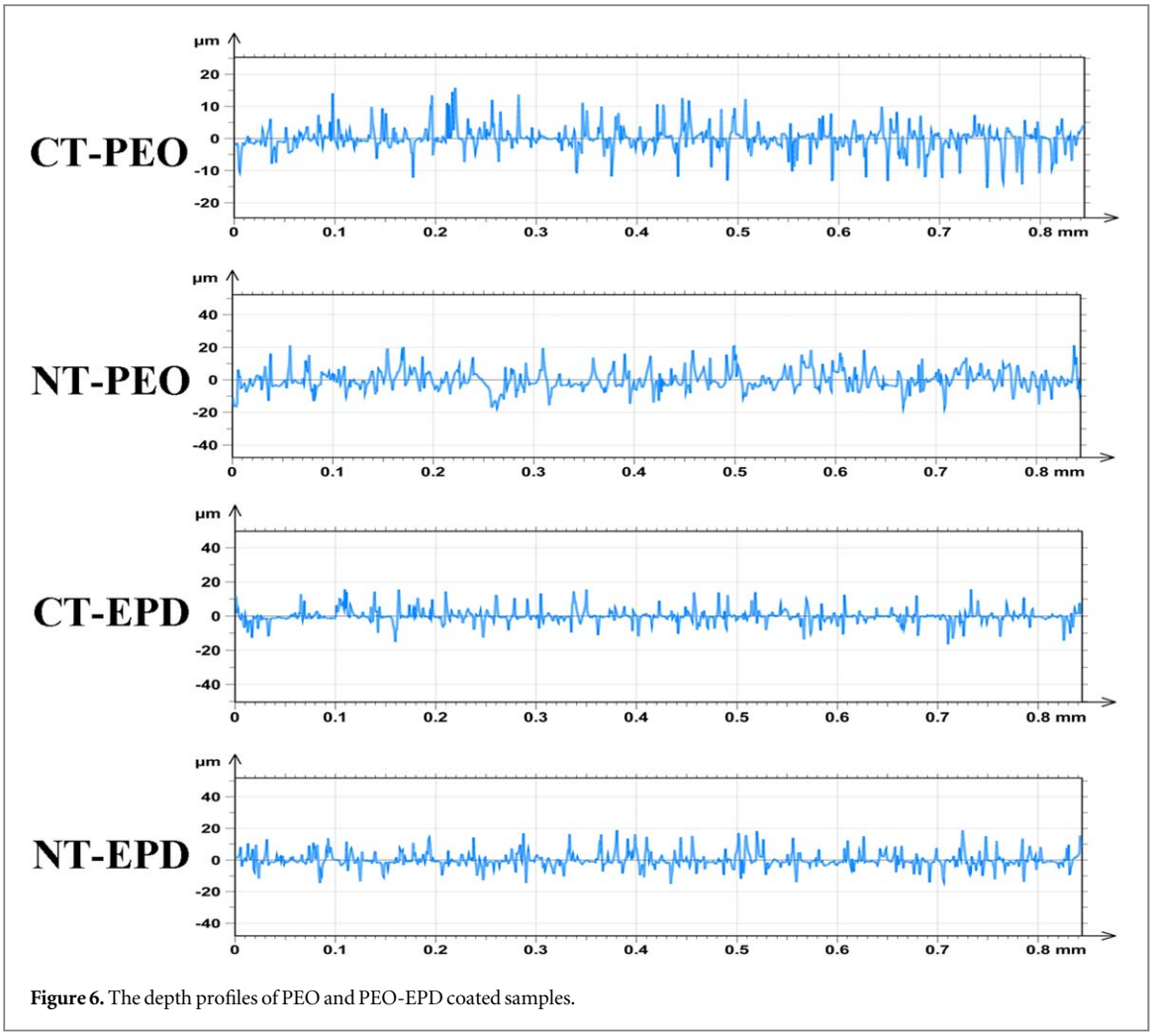

Figure 6. The depth profiles of PEO and PEO-EPD coated samples.

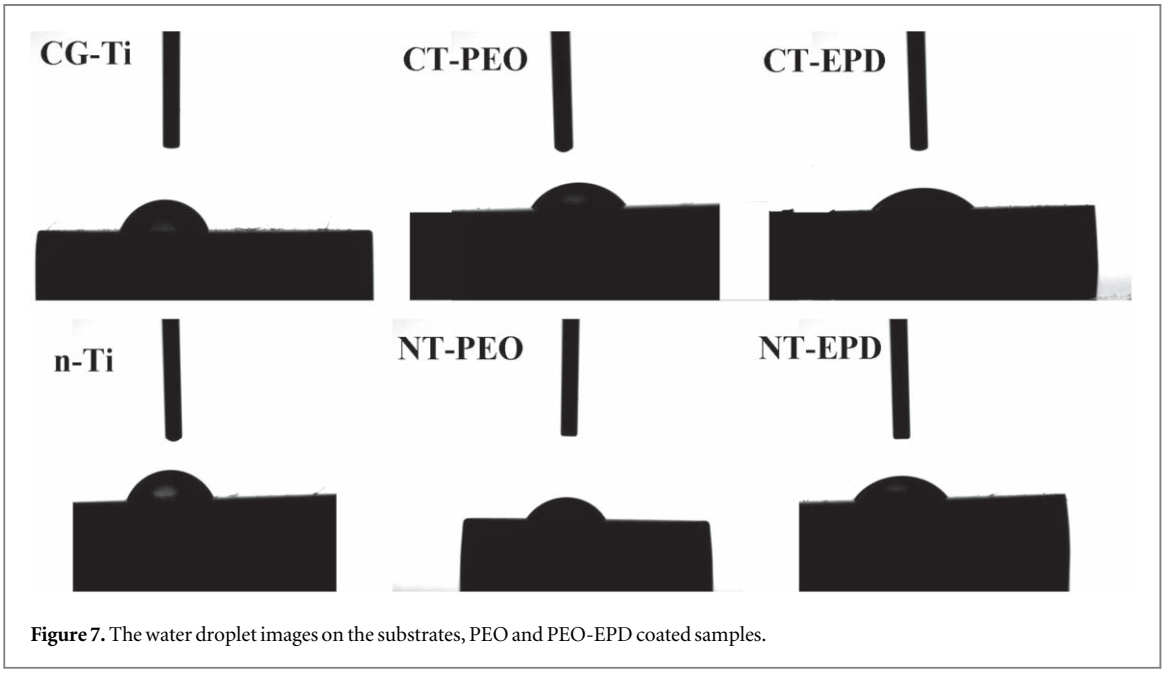

Figure 7. The water droplet images on the substrates, PEO and PEO-EPD coated samples.

the material homogeneity and formation of an effective passive layer at grain boundaries of nanostructured material [10, 11]. Additionally, n-Ti can produce a highly stable oxide layer with a superior grain boundary portion, playing a crucial role in shielding the material against corrosion [38]. All the coated samples showed higher E_{corr} and lowered i_{corr} values compared to CG-Ti and n-Ti, ascribed to a lower corrosion tendency of

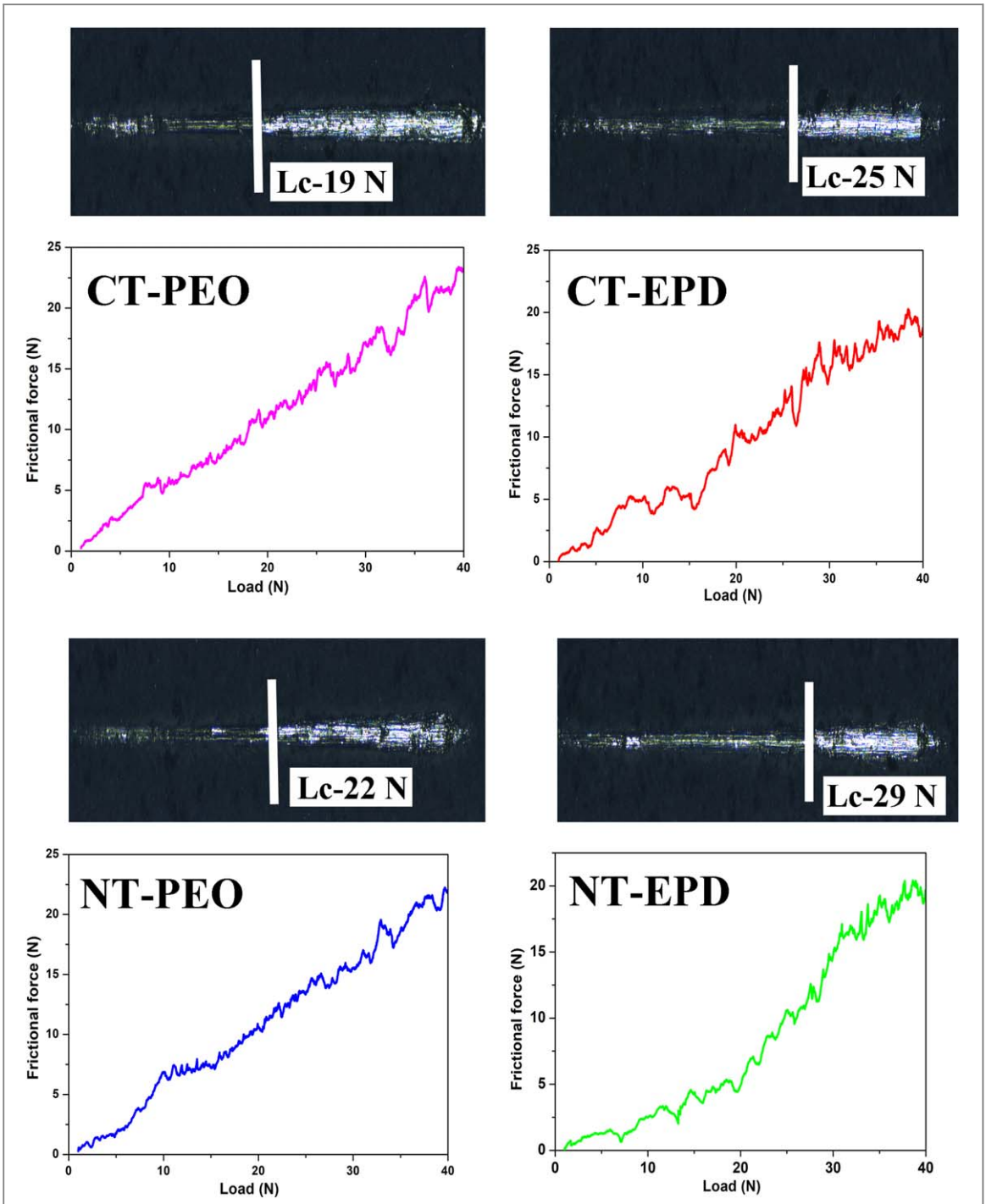

Figure 8. Friction force vs load curves and corresponding panoramic optical micrographs of the PEO and PEO-EPD coated samples.

Table 5. The contact angle (θ), surface energy (E_s) and critical load (L_c) of substrates (CG-Ti and N-Ti), PEO and PEO-EPD coated samples.

Sample code	θ (degrees)	E_s (mJ m^{-2})	L_c (N)
CG-Ti	74	20	—
CT-PEO	58	39	19
CT-EPD	44	52	25
n-Ti	71	24	—
NT-PEO	52	45	22
NT-EPD	40	56	29

coated samples than the substrate. The PEO-EPD (NT-EPD and CT-EPD) samples have shown higher E_{corr} and lower i_{corr} than PEO coated (NT-PEO and CT-PEO) samples. Among the four coatings, Ca and P containing TiO_2 developed on nanostructured titanium exhibited better corrosion resistance than coarse-grained titanium; it is mainly influenced by surface morphology along with the more compact and high thickness of the coatings produced on nanostructured titanium as evident from FESEM micrographs in figures 3 and 4.

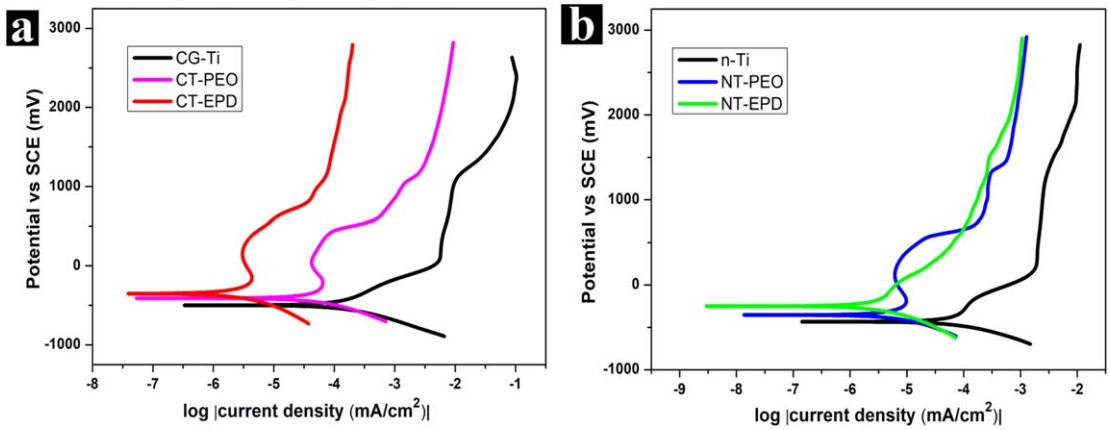

Figure 9. Potentiodynamic polarisation curves of (a) CG-Ti, CT-PEO and CT-EPD, (b) n-Ti, NT-PEO and NT-EPD.

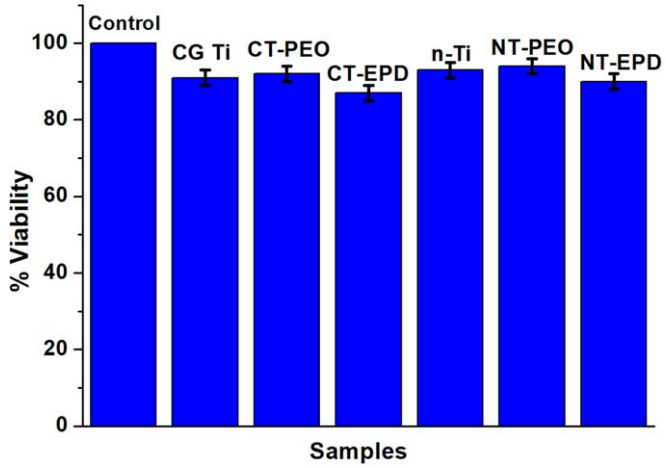

Figure 10. Percentage viability of cells on the substrates, PEO and PEO-EPD coated samples.

Table 6. The potentiodynamic polarisation parameters of coated samples and substrates in SBF medium.

Sample	E_{corr} versus SCE (mV)	i_{corr} (mA cm^{-2})
CG-Ti	−501.5	1.05×10^{-4}
CT-PEO	−401.2	2.93×10^{-5}
CT-EPD	−353.5	1.84×10^{-6}
n-Ti	−436.5	3.33×10^{-5}
NT-PEO	−355.9	3.85×10^{-6}
NT-EPD	−251.4	8.85×10^{-7}

3.8. *In vitro* assessment of cytotoxicity

3.8.1. MTT assay

Cytocompatibility of CG-Ti, n-Ti substrates, and coated samples can be evaluated using the MTT assay, which can quantify the percentage viability of L-929 fibroblast cells. The % viability of control, CG-Ti, n-Ti, CT-PEO, NT-PEO, CT-EPD, and NT-EPD samples are 100, 91, 93, 92, 94, 87, 90, respectively, and are depicted in figure 10. The MTT assay disclosed that cell viability of all the coated samples and substrates was reported above 85%, indicating the nontoxic nature of degradation products of titanium substrate, PEO and PEO-EPD coated samples [43]. The coatings consist of numerous pores on the surface, which can provide cellular communication efficiently and preserve the nutrients. The coarse-grained and nanostructured titanium PEO coated samples exhibited significantly higher percentage viability than the substrate and PEO-EPD samples. The samples CT-EPD and NT-EPD exhibited lower viability than CT-PEO and NT-PEO, attributed to the release of calcium ions in higher amounts due to the HA addition [20, 44].

3.8.2. Apoptosis test

The fluorescent images of the substrates and coated samples obtained from the apoptosis test reported the distribution of live and dead L-929 fibroblast cells. So, the cells with a green nucleus are live cells, and cells that appear as orange has undergone necrotic or apoptosis, whereas red cells represent dead cells [20]. Fluorescent images of titanium substrates, control, and coated samples CT-PEO, NT-PEO, CT-EPD and NT-EPD are depicted in figure 11. These images show that the samples have exhibited a green nucleus, and captured images agree with MTT assay results. The

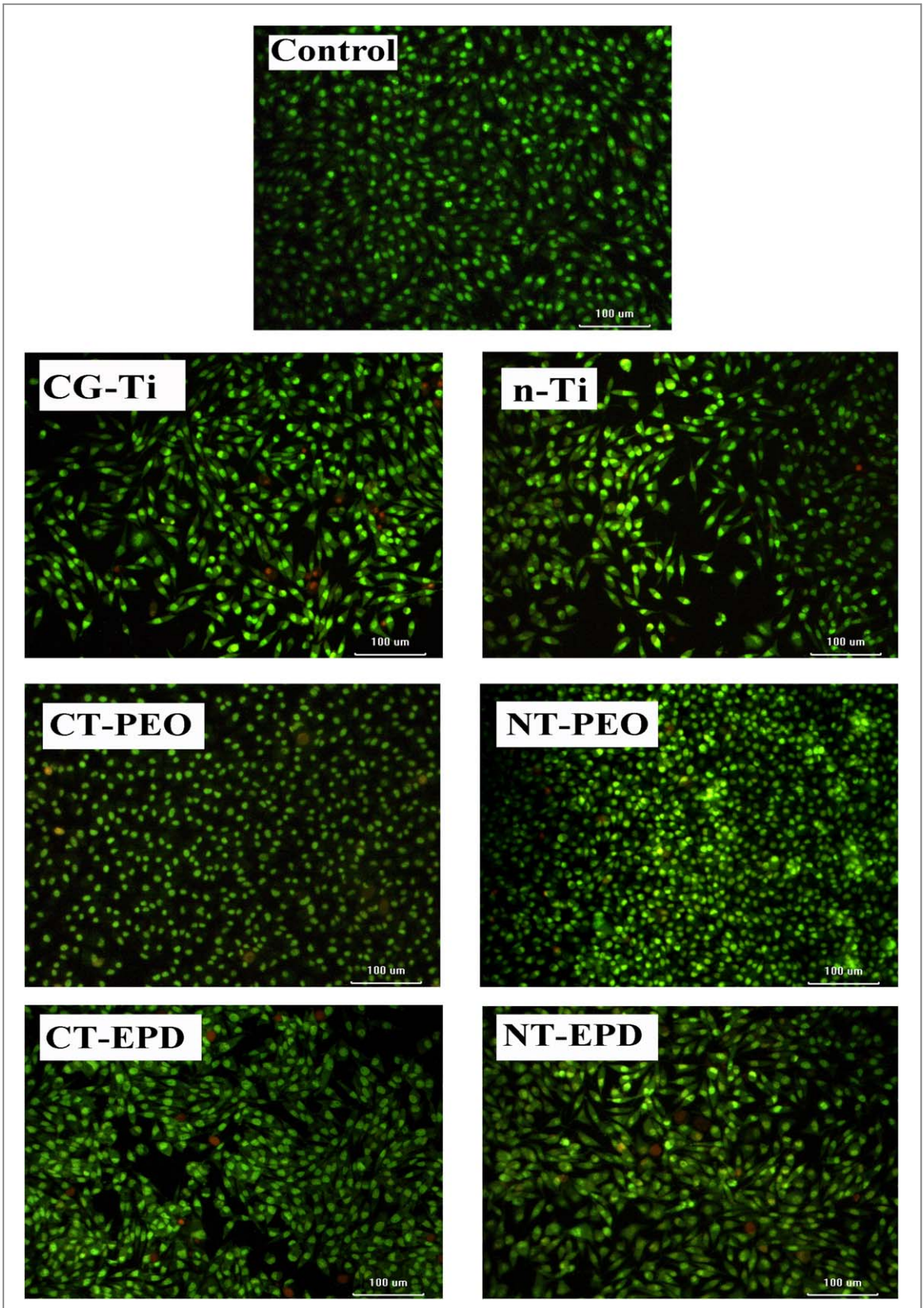

Figure 11. Epifluorescent images of L-929 fibroblast cells on the substrates, PEO and PEO-EPD coated samples.

PEO coated samples demonstrated all live cells without any necrotic cells. The PEO-EPD samples showed a green nucleus with an elongated structure and a significantly negligible number of necrotic cells; attributed to the cells present on these samples were proliferating and healthy, even though the MTT assay values are lower than that of the PEO treated samples. The apoptosis test reveals that PEO-EPD coating features of coarse-grained and nanostructured titanium in the phosphate-based electrolyte system may acquire the required nutrients and promote cell growth on the surface [45, 46].

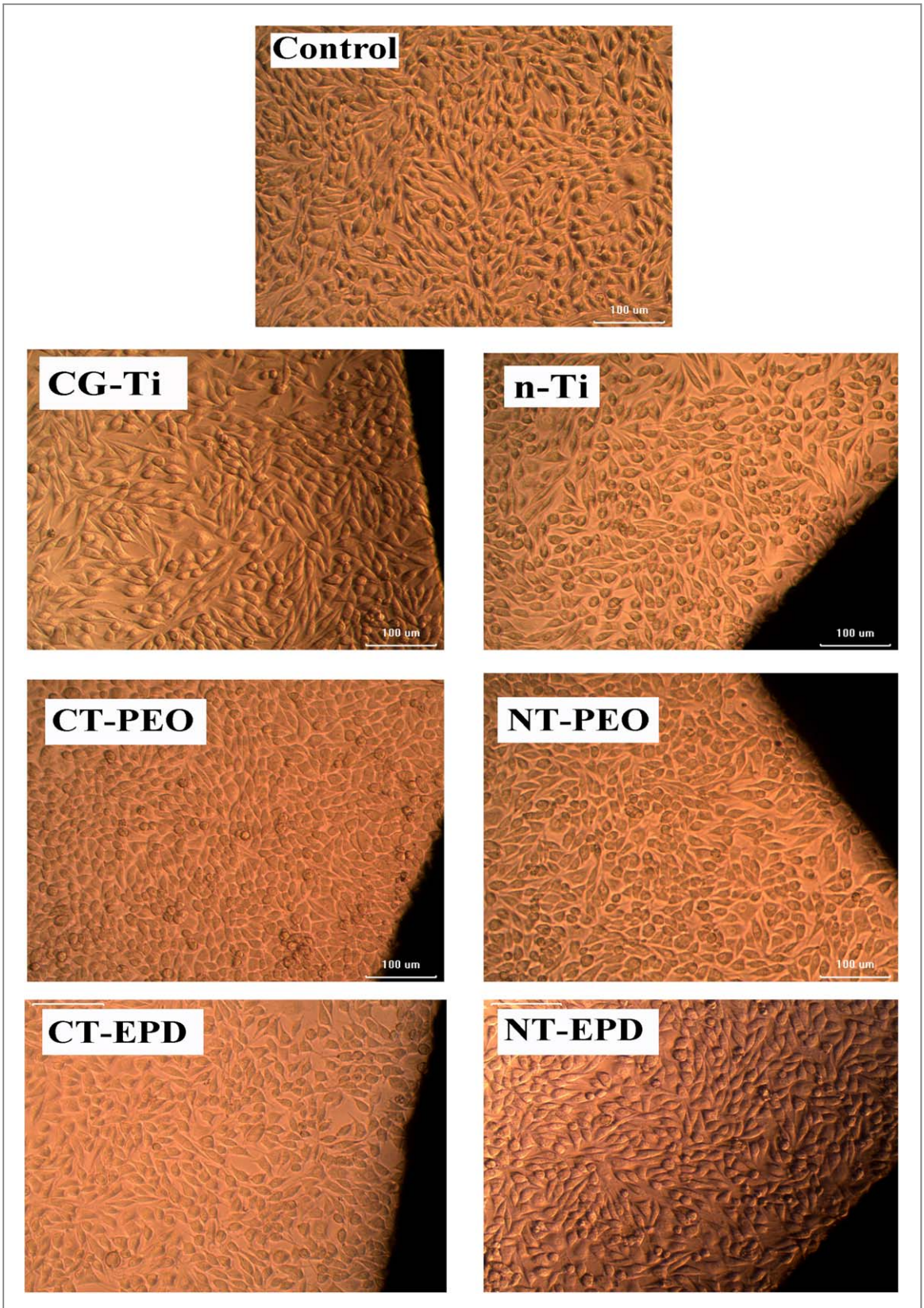

Figure 12. Phase contrast image of L-929 fibroblast cells on the substrates, PEO and PEO-EPD coated samples.

3.8.3. Direct contact assay

The direct contact assay assesses the L-929 cell adherence and proliferation around the titanium substrates (CG-Ti and n-Ti) along with the coated samples (CT-PEO, NT-PEO, CT-EPD and NT-EPD). A phase-contrast microscope captured the morphology of the cells, and the respective images are depicted in figure 12. The sample will appear by black colour in the reported images, and the seeded cells with growth medium surrounding the sample will appear in orange colour. It is curious to observe that the L-929 cells prefer to proliferate and adhere to the interface. The interface between the sample

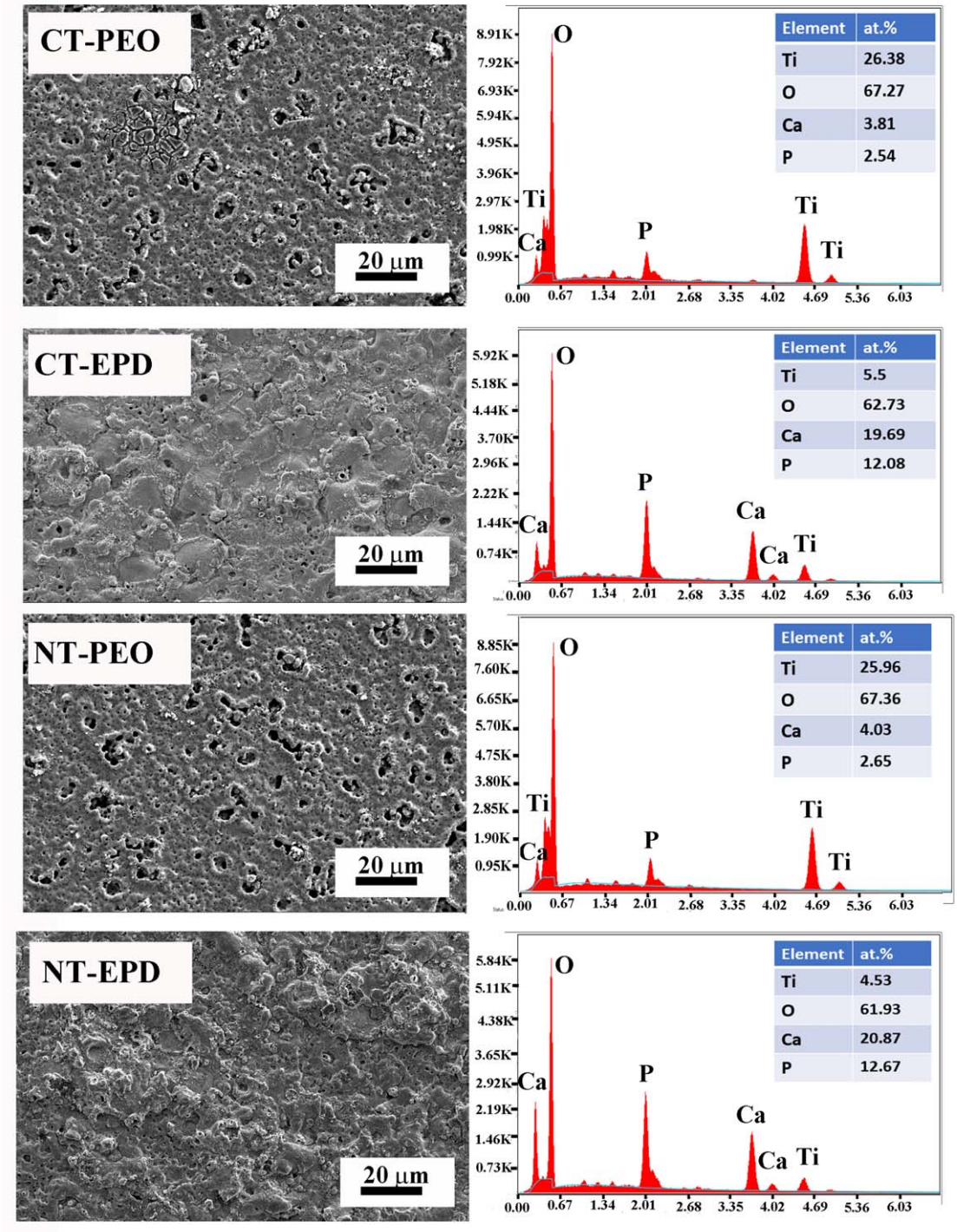

Figure13. FESEM surface morphology and corresponding EDS spectra of the PEO and PEO-EPD fabricated samples after immersion in 7.4 pH SBF solution for 14 days.

and seeded cells becomes a seductive destination for L-929 cell growth, which is mainly owing to the porous structure present on the samples. This porous structure will provide nutrients to the growing cells [43]. It is clearly observed that adherence and growth of L-929 cells are higher on coated samples compared to the untreated titanium substrates. Among all the coated samples, the PEO-EPD coated coarse-grained, and nanostructured titanium samples provided a more supportive microenvironment for cell growth.

3.9. *In-vitro* bioactivity study

The orthopaedic and dental implant surfaces should accelerate the new bone formation and bond with existing bone throughout the implantation period [47]. The coated samples (PEO and PEO -EPD treated samples) were immersed in a 7.4 pH SBF medium for 14 days to examine the apatite growth. After 14 days, the SBF immersed samples surface morphology was analysed by FESEM to evaluate apatite growth on the surface. The surface morphology and elemental

composition of the sample are reported in figure13. From figure13, we can observe no noticeable changes in surface morphology of PEO coated samples even after immersion for 14 days. The EDS results of CT-PEO and NT-PEO coatings show the presence of Ca and P elements with Ca/P ratios of 1.50 and 1.52, respectively, much lower than stoichiometric hydroxyapatite (Ca/P ratio of 1.67). On the other hand, the PEO-EPD coated samples exhibited significant surface morphology changes with uniform apatite layer depositions that can be observed throughout the surface. The PEO-EPD samples also have strong signals of Ca and P with Ca/P ratio of CT-EPD and NT-EPD coated samples of 1.63 and 1.65, indicating its bioactivity. The PEO-EPD treated samples have a higher bioactivity than the PEO treated samples, characterised by apatite formation on the whole surface and its composition.

4. Conclusions

In the present study, Ca and P containing TiO_2 bioceramic coatings on coarse-grained and nanostructured CP-Ti were successfully produced by PEO and PEO-EPD processes, a comprehensive study of their architecture and properties was performed, and the following major findings were obtained.

1. The presence of TiO_2 oxide films with anatase and rutile phases was confirmed by XRD analysis. PEO-EPD coatings on both CG-Ti and n-Ti exhibited higher thickness and compactness as compared to the PEO coatings. The presence of Ca and P elements in PEO-EPD coatings was significantly higher.
2. The NT-EPD sample exhibited high surface roughness ($2.51 \pm 0.1\ \mu$m) and a lower contact angle (40°) to attain higher cell viability. Meanwhile, PEO-EPD samples exhibited superior corrosion resistance than PEO samples. NT-EPD sample has the lowest corrosion current density (8.85×10^{-7} mA cm^{-2}) among the coated samples indicating its higher corrosion resistance. The obtained data clearly indicate the importance of the effect of nanostructure in the substrate on the structure and properties of the coatings.
3. Cytocompatibility of the L-929 fibroblast cells on both CG-Ti and n-Ti substrates, along with coated samples, are established by apoptosis and MTT assay. PEO-EPD coated sample exhibited a green nucleus with an elongated structure, ascribed to higher cell growth than the substrate and PEO coated sample.
4. The PEO-EPD coatings on both CG-Ti and n-Ti samples exhibited good bioactivity by forming a bone-like apatite layer within 14 days in a 7.4 pH SBF medium.

Acknowledgments

The authors are grateful to the Department of Science & Technology (DST), New Delhi, India, through grant No DST/INT/RUS/RSF/P-35 and the Russian Science Foundation (RSF), Moscow, Russia, through grant No. 19-49-02003 to carry out this work.

Data availability statement

All data that support the findings of this study are included within the article (and any supplementary files).

ORCID iDs

Rameshbabu N https://orcid.org/0000-0001-7290-287X

References

[1] Liao S-C, Chang CT, Chen CY, Lee CH and Lin WL 2020 Functionalisation of pure titanium MAO coatings by surface modifications for biomedical applications *Surf. Coat. Technol.* **394** 125812
[2] Pesode P A and Barve S B 2021 Recent advances on the antibacterial coating on titanium implant by micro-Arc oxidation process *Mater. Today Proc.* **47** 5652–62
[3] Rameshbabu N, Ravisankar B, Saikiran A, Parfenov E V and Valiev R Z 2019 Surface modification of CP-Ti metallic implant material by plasma electrolytic oxidation *Mater. Sci. Eng.* **672** 012012
[4] Dyakonov G S, Mironov S, Semenova I P, Valiev R Z and Semiatin S L 2017 Microstructure evolution and strengthening mechanisms in commercial-purity titanium subjected to equal-channel angular pressing *Mater. Sci. Eng.* A **701** 289–301
[5] Valiev R Z, Parfenov E V and Parfenova L V 2019 Developing nanostructured metals for manufacturing of medical implants with improved design and biofunctionality *Mater. Trans.* **60** 1356–66
[6] Valiev R Z, Prokofiev E A, Kazarinov N A, Raab G I, Minasov T B and Strasky J 2020 Developing nanostructured Ti Alloys for innovative implantable medical devices *Mater.* **13** 967
[7] Elias C N, Meyers M A, Valiev R Z and Monteiro S N 2013 Ultrafine grained titanium for biomedical applications: an overview of performance *J. Mater. Res. Technol.* **2** 340–50
[8] Ravisankar B, Rameshbabu N, Parfenov E V and Valiev R Z 2021 Development of nanostructured titanium implants for biomedical implants—a short review *Mater. Today Proc.* **46** 1198–200
[9] Polyakov A V, Dluhos L, Dyakonov G S, Raab G I and Valiev R Z 2015 Recent advances in processing and application of nanostructured titanium for dental Implants *Adv. Eng. Mater.* **17** 1869–75
[10] Attarilar S, Djavanroodi F, Irfan O M, Al-Mufadi F A, Ebrahimi M and Wang Q D 2020 Strain uniformity footprint on mechanical performance and erosion corrosion behavior of equal channel angular pressed pure titanium *Results Phy.* **17** 103141
[11] Gu Y, Ma A, Jiang J, Li H, Song D, Wu H and Yuan Y 2018 Simultaneously improving mechanical properties and corrosion resistance of pure Ti by continuous ECAP plus short-duration annealing *Mater. Charact.* **138** 38–47
[12] Kim H S, Yoo S J, Ahn J W, Kim D H and Kim W J 2011 Ultrafine grained titanium sheets with high strength and high corrosion resistance *Mater. Sci. Eng.* A **528** 8479–85

[13] Fattah-Alhosseini A, Ansari A R, Mazaheri Y and Keshavarz M K 2017 Effect of immersion time on the passive and electrochemical response of annealed and nano-grained commercial pure titanium in Ringer's physiological solution at 37 °C *Mater. Sci. Eng.* C **71** 771–9
[14] Biguetti C C *et al* 2021 Effects of titanium corrosion products on *in vivo* biological response: a basis for the understanding of osseointegration failures mechanisms *Front. Mater.* **8** 651970
[15] Saikiran A, Hariprasad S, Manojkumar P, Rama Krishna L and Rameshbabu N 2020 Effect of laser treatment on morphology and corrosion behaviour of the plasma electrolytic oxidation coatings developed on aluminised steel *Surf. Coat. Technol.* **394** 125888
[16] Semenova I P, Valiev R Z, Smyslov A M, Pesin M V and Langdon T G 2021 Advanced materials for mechanical engineering: ultrafine-grained alloys with multilayer coatings *Adv. Eng. Mater.* **23** 2100145
[17] Hariprasad S, Gowtham S, Arun S, Ashok M and Rameshbabu N 2017 Fabrication of duplex coatings on biodegradable AZ31 magnesium alloy by integrating cerium conversion (CC) and plasma electrolytic oxidation (PEO) processes *J. Alloy Compd.* **722** 698–715
[18] Pereira B L, da Luz A R, Lepienski C M, Mazzaro I and Kuromoto N K 2018 Niobium treated by plasma electrolytic oxidation with calcium and phosphorus electrolytes *J. Mech. Behav. Biomed. Mater.* **77** 347–52
[19] Zhu L, Ke X, Li J, Zhang Y, Zhang Z and Sui M 2021 Growth mechanisms for initial stages of plasma electrolytic oxidation coating on Al *Surf. Interfaces* **25** 101186
[20] Lokeshkumar E, Manojkumar P, Saikiran A, Premchand C, Hariprasad S, Rama Krishna L and Rameshbabu N 2021 Fabrication of Ca and P containing niobium oxide ceramic coatings on niobium by PEO coupled EPD process *Surf. Coat. Technol.* **416** 127161
[21] Babaei K, Fattah-Alhosseini A and Chaharmahali R 2020 A review on plasma electrolytic oxidation (PEO) of niobium: mechanism, properties and applications *Surf. Interfaces* **21** 100719
[22] Manojkumar P, Lokeshkumar E, Saikiran A, Govardhanan B, Ashok M and Rameshbabu N 2020 Visible light photocatalytic activity of metal (Mo/V/W) doped porous TiO_2 coating fabricated on CP-Ti by plasma electrolytic oxidation *J. Alloy Compd.* **825** 154092
[23] Xu L, Wu C, Lei X, Zhang K, Liu C, Ding J and Shi X 2018 Effect of oxidation time on cytocompatibility of ultrafine-grained pure Ti in micro-arc oxidation treatment *Surf. Coat. Technol.* **342** 12–22
[24] Yao Z Q, Ivanisenko Y, Diemant T, Caron A, Chuvilin A, Jiang J Z, Valiev R Z, Qi M and Fecht H J 2010 Synthesis and properties of hydroxyapatite-containing porous titania coating on ultrafine-grained titanium by micro-arc oxidation *Acta Biomater.* **6** 2816–25
[25] Nazarov D, Zemtsova E, Smirnov V, Mitrofanov I, Maximov M, Yudintceva N and Shevtsov M 2021 The effects of chemical etching and ultra-fine grain structure of titanium on MG-63 cells response *Metals* **11** 510
[26] Sandhyarani M, Rameshbabu N, Venkateswarlu K and Rama Krishna L 2014 Fabrication, characterisation and *in-vitro* evaluation of nanostructured zirconia/hydroxyapatite composite film on zirconium *Surf. Coat. Technol.* **238** 58–67
[27] Qing F, Wang Z, Hong Y, Liu M, Guo B, Luo H and Zhang X 2012 Selective effects of hydroxyapatite nanoparticles on osteosarcoma cells and osteoblasts *J. Mater. Sci., Mater. Med.* **23** 2245–51
[28] Moskalewicz T, Warcaba M, Cieniek L, Sitarz M, Gajewska M and Boccaccini A R 2021 Hydroxyapatite/sodium alginate coatings electrophoretically deposited on titanium substrates: microstructure and properties *Appl. Surf. Sci.* **540** 148353
[29] Qadir M, Li Y, Biesiekierski A and Wen C 2021 Surface Characterisation and biocompatibility of hydroxyapatite coating on anodised TiO_2 nanotubes via PVD magnetron sputtering *Langmuir* **37** 4984–96
[30] Liu B, Yu W, Xiao G, Chen C and Lu Y 2021 Comparative investigation of hydroxyapatite coatings formed on titanium via phosphate chemical conversion *Surf. Coat. Technol.* **413** 127093
[31] Bordbar-Khiabani A, Bahrampour S, Mozafari M and Gasik M 2022 Surface functionalisation of anodised tantalum with Mn_3O_4 nanoparticles for effective corrosion protection in simulated inflammatory condition *Ceram. Int.* **48** 3148–56
[32] Bordbar-Khiabani A, Rahimi S, Yarmand B and Mozafari M 2018 Electrophoretic deposition of graphene oxide on plasma electrolytic oxidised-magnesium implants for bone tissue engineering applications *Mater. Today Proc.* **5** 15603–12
[33] Bordbar-Khiabani A, Yarmand B and Mozafari M 2020 Effect of ZnO pore-sealing layer on anti-corrosion and *in-vitro* bioactivity behavior of plasma electrolytic oxidised AZ91 magnesium alloy *Mater. Lett.* **258** 126779
[34] Valiev R Z, Semenova I P, Latysh V V, Shcherbakov A V and Yakushina E B 2008 Nanostructured titanium for biomedical applications: new developments and challenges for commercialisation *Nanotechnologies Russ.* **3** 593–601
[35] Ikonopisov S, Girginov A and Machkova M 1979 Electrical breaking down of barrier anodic films during their formation *Electrochim. Acta* **24** 451–6
[36] Venkateswarlu K, Rameshbabu N, Sreekanth D, Bose A C, Muthupandi V, Babu N K and Subramanian S 2012 Role of electrolyte additives on *in-vitro* electrochemical behavior of micro arc oxidised titania films on Cp Ti *Appl. Surf. Sci.* **258** 6853–63
[37] He J, Zhou W, Zhou X, Zhong X, Zhang X, Wan P, Zhu B and Chen W 2008 The anatase phase of nanotopography titania plays an important role on osteoblast cell morphology and proliferation *J. Mater. Sci. Mater. Med.* **19** 3465–72
[38] Reshadi F, Faraji G, Baniassadi M and Tajeddini M 2017 Surface modification of severe plastically deformed ultrafine grained pure titanium by plasma electrolytic oxidation *Surf. Coat. Technol.* **316** 113–21
[39] Hariprasad S, Saikiran A, Premchand C, Rama Krishna L and Rameshbabu N 2021 Fabrication of ceramic coatings on the biodegradable ZM21 magnesium alloy by PEO coupled EPD followed by laser texturing process *J. Magnes. Alloy.* **9** 910–26
[40] Masrouri M, Faraji G, Pedram M S and Sadrkhah M 2020 *In-vivo* study of ultrafine-grained CP-Ti dental implants surface modified by SLActive with excellent wettability *Int. J. Adhes. Adhes.* **102** 102684
[41] Gowtham S, Hariprasad S, Arunnellaiappan T and Rameshbabu N 2017 An investigation on ZrO_2 nano-particle incorporation, surface properties and electrochemical corrosion behaviour of PEO coating formed on CP-Ti *Surf. Coat. Technol.* **313** 263–73
[42] Wang C T, Escudeiro A, Polcar T, Cavaleiro A, Wood R J K, Gao N and Langdon T G 2013 Indentation and scratch testing of DLC-Zr coatings on ultrafine-grained titanium processed by high-pressure torsion *Wear* **306** 304–10
[43] Rizal U, Swain B S, Rameshbabu N and Swain B P 2018 Biocompatibility of hydrogen-diluted amorphous silicon carbide thin films for artificial heart valve coating *J. Mater. Eng. Perform.* **27** 2679–86
[44] Maeno S, Niki Y, Matsumoto H, Morioka H, Yatabe T, Funayama A, Toyama Y, Taguchi T and Tanaka J 2005 The effect of calcium ion concentration on osteoblast viability, proliferation and differentiation in monolayer and 3D culture *Biomaterials* **26** 4847–55
[45] Amaravathy P, Sowndarya S, Sathyanarayanan S and Rajendran N 2014 Novel sol-gel coating of Nb_2O_5 on magnesium alloy for biomedical applications *Surf. Coat. Technol.* **244** 131–41
[46] Thankam F G and Muthu J 2014 Influence of physical and mechanical properties of amphiphilic biosynthetic hydrogels on long-term cell viability *J. Mech. Behav. Biomed. Mater.* **35** 111–22
[47] Sandhyarani M, Prasadrao T and Rameshbabu N 2014 Role of electrolyte composition on structural, morphological and *in-vitro* biological properties of plasma electrolytic oxidation films formed on zirconium *Appl. Surf. Sci.* **317** 198–209